arXiv:2603.23179v2 [cs.CV] 3 Aug 2026

Gimbal360: Canonicalizing Planar Diffusion for Spherical Panorama Completion

Yuqin Lu Haofeng Liu Yang Zhou Yihua Dai Guiqing Li Shengfeng He Jun Liang

https://orange-3dv-team.github.io/Gimbal360

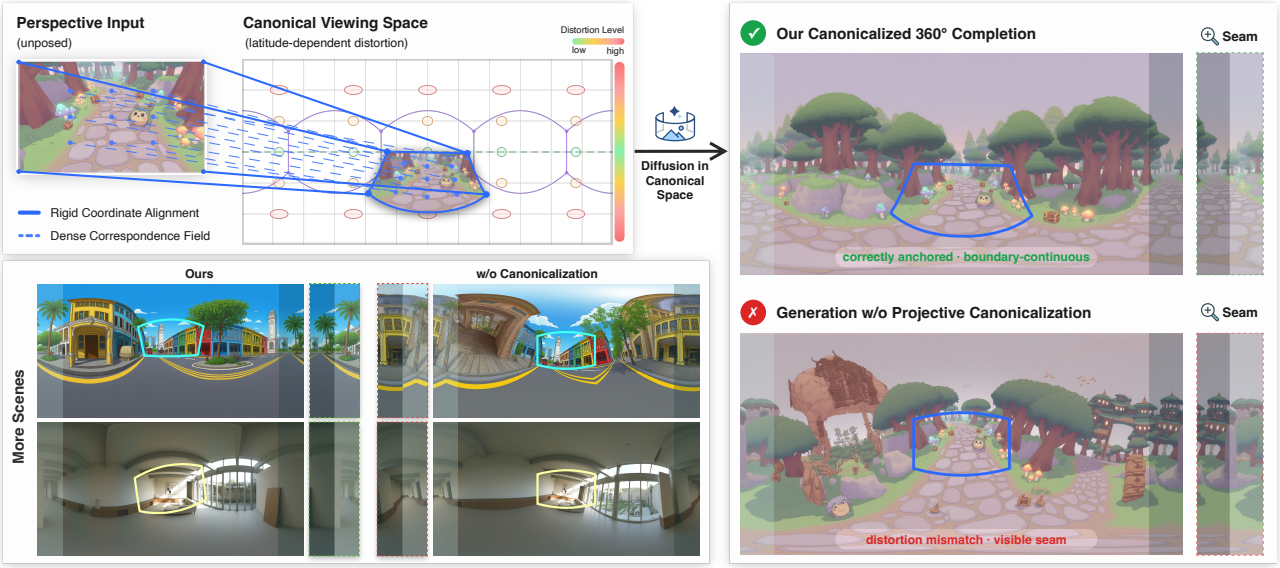


Figure 1. We present **Gimbal360**, a unified framework for completing a full 360° panorama from a single unposed perspective image. Directly applying planar diffusion priors without canonicalization leads to mismatched geometric distortions and visible discontinuities at the panoramic boundary. Gimbal360 resolves these incompatibilities in a canonical spherical representation, producing structurally coherent and seamless panoramic completions. Please zoom in for a better view.

Abstract

Diffusion models provide powerful priors for 2D image completion, but these priors are learned on bounded planar images and do not transfer directly to 360° panoramas. Perspective observations and spherical panoramas differ in both projective geometry and topology: viewpoint-dependent distortion complicates spatial correspondence, while Equirectangular Projection (ERP) panoramas exhibit intrinsic S^1 periodicity that standard Euclidean architectures do not preserve. We present Gimbal360*, a unified framework that adapts planar diffusion priors to spherical panoramic completion by standardizing these geometric and topological structures. Our Canonical Viewing Space expresses projective distortion as a fixed function of latitude, providing a consistent interface between perspective inputs and spherical panoramas. To map unposed in-the-wild images into this space, Differentiable Projective Canonicalization projects a dense correspondence field onto a 3-DoF rigid projection manifold without requiring camera parameters at inference. We further introduce Topologically Equivariant Generation, which enforces latent shift equivariance to preserve continuity across the periodic ERP boundary. Together, these designs allow diffusion to operate in a representation whose geometry and topology are explicitly aligned with the spherical domain. We also introduce Horizon360, a curated large-scale dataset of gravity-aligned panoramic environments. Extensive experiments show that Gimbal360 achieves state-of-the-art visual fidelity and seam continuity in 360° scene completion.*

1. Introduction

The advent of large-scale diffusion models [36] has catalyzed major advances in generative computer vision, par-

ticularly in image outpainting and completion [31, 56]. Extending these models to 360° panoramic completion promises immersive content creation for world generation, virtual reality, and image-based lighting [18, 46], yet remains fundamentally challenging. Because high-quality omnidirectional data remain scarce relative to perspective imagery, the prevailing paradigm reuses pre-trained planar diffusion priors [25, 36] for panoramic completion. However, this reuse exposes a fundamental mismatch: such priors are learned on bounded Euclidean grids ($\mathbb{R}^2$), whereas a panorama lies on the spherical manifold (S^2), parameterized by equirectangular projection (ERP). We argue that the recurring failure modes of omnidirectional completion, including structural collapse, architectural hallucination, and boundary seams, trace back to two unresolved domain gaps.

The first gap arises from *projective variance*. An unposed perspective image is captured under unknown viewing geometry, so its projection onto the ERP canvas induces distortions that vary with the unknown pose: straight architectural lines become sinusoidal curves whose shape cannot be anticipated by the prior, violating the Manhattan-world regularities it has internalized. Existing pipelines sidestep this by assuming leveled inputs or ground-truth viewing parameters [18, 30, 48, 57], which limits real-world applicability. Learning the alignment implicitly with a spatial transformer [19] is notoriously unstable because the diffusion objective propagates high-frequency, pixel-level gradients that push a free-form warper toward non-rigid, "jelly-like" deformations rather than a coherent global alignment.

The second gap stems from *topological severing*. ERP is periodic along the azimuth since its left and right borders depict the same physical location on the S^1 boundary. Standard generative architectures, however, assume a bounded Euclidean plane. For example, zero-padding in the VAE injects artificial borders that terminate the canvas at the seam, while absolute positional encodings in diffusion transformers treat opposite borders as maximally distant. Both mechanisms sever the periodic structure of ERP. Prior work mitigates this through inference-time remedies such as circular blending [11] or synchronized multi-view denoising [26]. These post-hoc corrections fundamentally behave as spatial low-pass filters. While they reduce visible seams, they smooth high-frequency details and cannot resolve the underlying topological mismatch.

In this work, we present **Gimbal360**, which bridges both gaps through a single design philosophy: *canonicalization*. Our key observation is that once a scene is anchored to a gravity-aligned, canonical reference frame, ERP distortion no longer depends on the unknown viewing geometry and reduces to a fixed, predictable function of latitude. Gimbal360 therefore canonicalizes at three levels. At the data level, we curate *Horizon360*, a large-scale collection of gravity-aligned panoramic environments that establishes a clean canonical structural prior. At the geometric level, a Differentiable Projective Canonicalization (DPC) module anchors unposed inputs into the Canonical Viewing Space. It predicts a dense correspondence field from input pixels to the ERP canvas and collapses it, through a differentiable rigid solver, onto a 3-DoF rigid projection manifold. This rigid bottleneck filters noisy diffusion gradients into globally coherent alignment updates, enabling stable joint training with the generator while requiring no pose annotations at inference. At the topological level, we address the Euclidean boundary assumption by enforcing topological equivariance directly within the generative pipeline. Our Topologically Equivariant Generation (TEG) combines circular latent encoding with a Siamese shift-equivariance objective that penalizes inconsistency under azimuthal shifts, teaching the generator to respect the intrinsic S^1 periodic structure of panoramic imagery. This design preserves boundary continuity at the architectural level and substantially reduces seam artifacts during generation.

In summary, our contributions are threefold:

- We identify the geometric and topological domain gaps between planar diffusion priors and the spherical manifold, and introduce a Canonical Viewing Space together with a large-scale gravity-aligned dataset, Horizon360, to establish a unified structural prior.
- We propose Differentiable Projective Canonicalization, which regularizes geometric alignment by constraining dense correspondences to a rigid transformation via a differentiable rigid bottleneck, stabilizing joint training with the generator without pose annotations at inference.
- We enforce topological equivariance in the generative pipeline through circular latent encoding and Siamese shift-equivariant training, enabling diffusion models to respect the intrinsic S^1 periodicity of panoramic imagery.

2. Related Work

Image Outpainting and Completion. Image outpainting extrapolates content beyond the original boundaries while preserving semantic and structural consistency. Early approaches relied on GANs [12] to hallucinate missing regions [45, 55, 56], and diffusion models have since brought substantial gains in fidelity and coherence [9, 31, 36], with latent diffusion enabling flexible conditioning on image and text prompts. These approaches, however, are inherently designed for planar images on Euclidean grids ($\mathbb{R}^2$); applied directly to omnidirectional extrapolation, they struggle with the distortions and closed-loop topology of spherical panoramas, producing structural inconsistencies and semantic drift as the field of view expands.

360° Panorama Generation. Panoramic generation has progressed from GAN-based systems [1, 6, 32] to diffusion frameworks for text-to-panorama synthesis [11, 27],

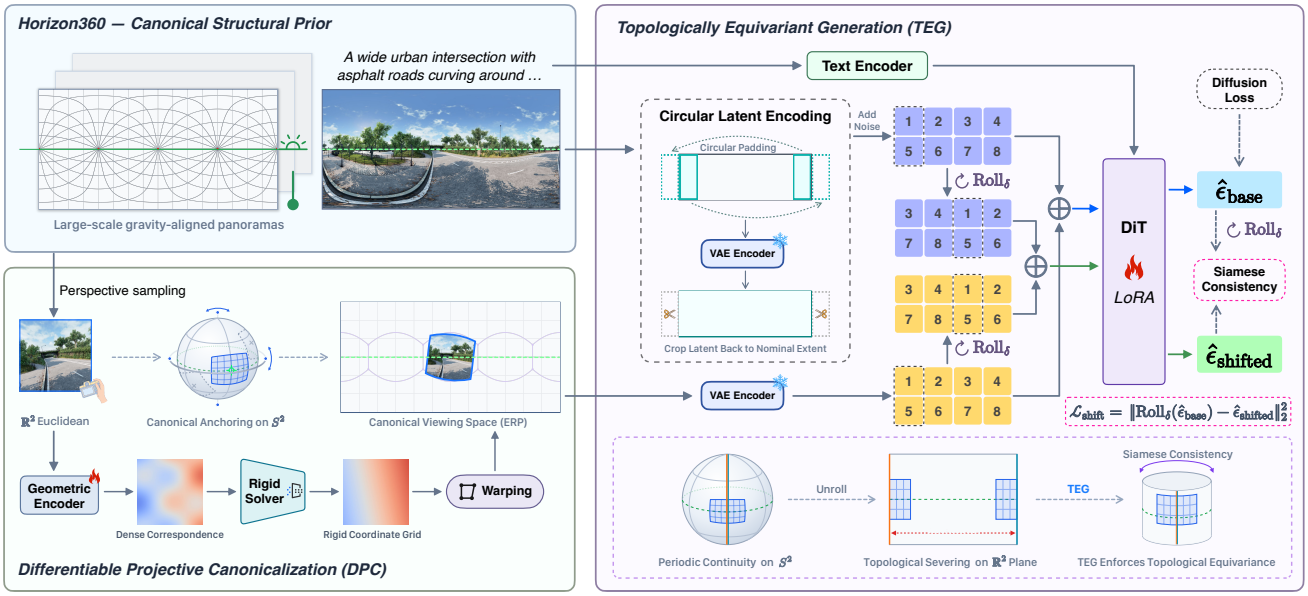


Figure 2. Overview of Gimbal360. Perspective views are sampled from Horizon360, our gravity-aligned canonical structural prior (top left). Differentiable Projective Canonicalization (DPC, bottom left) feeds the perspective input through a geometric encoder to predict a dense correspondence field, which the rigid solver collapses into a rigid coordinate grid that warps the view into the Canonical Viewing Space. Topologically Equivariant Generation (TEG, right) denoises in this space, where circular latent encoding wraps the frozen VAE via circular-padding and cropping, and a Siamese consistency loss aligns the predictions of the base and circularly shifted streams of a shared DiT. Together these mechanisms teach the generator to respect the periodic S^1 boundary (bottom right), ensuring structurally consistent and seamless panorama completions.

with dual-branch [53] and correspondence-aware [29] designs improving structural consistency. Extending a single narrow field-of-view image to a full panorama is more constrained: most diffusion-based outpainting pipelines [10, 18, 30, 39, 48, 57] project the input onto the ERP canvas using predefined viewing parameters, implicitly assuming gravity-aligned inputs, which limits their applicability to unconstrained captures [41]. Closest to our setting, CamFreeDiff [52] removes this assumption by regressing the input's spherical placement as a one-shot prediction within the diffusion pipeline. In contrast, our DPC module couples a dense correspondence field with a differentiable rigid solver, a bottleneck that both regularizes the placement estimate and permits stable joint training with the generative objective.

Geometric Adaptations in Omnidirectional Vision. Unlike perspective images, ERP panoramas exhibit severe latitude-dependent distortion and require continuity across the periodic boundary. Prior work adapts to the distortion either by modifying network operators, such as spherical convolutions [8], manifold-guided diffusion [40], and geometry-aware attention [47], or by reparameterizing the sphere into cubemaps [17, 22] and tangent planes [4]. Boundary continuity is likewise addressed through cylindrical convolutions [28] or inference-time corrections such as circular blending [11], synchronized denoising [26], and circular padding [44], which reduce visible seams but act as post-hoc low-pass corrections. Ensuring strict topological equivariance within the generative modeling process itself remains an open challenge.

3. Gimbal360

Given an unposed, narrow field-of-view (NFoV) perspective image $I_p \in \mathbb{R}^{H_p \times W_p \times 3}$, our goal is to synthesize a structurally coherent 360° ERP panorama $I_e \in \mathbb{R}^{H_e \times W_e \times 3}$. This task is fundamentally ill-posed: projecting an unposed I_p onto the spherical S^2 manifold induces severe non-linear distortions that violate the Euclidean ($\mathbb{R}^2$) structural priors of pre-trained diffusion models. To bridge planar diffusion priors and spherical panoramas, we propose Gimbal360. Instead of forcing the network to implicitly resolve arbitrary projective mappings, we introduce a Canonical Viewing Space, a gravity-aligned spherical coordinate system supported by our newly curated Horizon360 dataset, and resolve the domain gaps through two mechanisms. A Differentiable Projective Canonicalization (DPC) module recovers the spherical placement of the input and anchors its features into the canonical space through a rigid bottleneck, and a Topologically Equivariant Generation (TEG) scheme

preserves the periodic boundary of the panorama during diffusion. Fig. 2 provides an overview.

3.1. Preliminaries

Latent Diffusion Models (LDMs) [36] operate in the compressed latent space of a pre-trained autoencoder. An encoder $\mathcal{E}$ maps an image x to a spatial latent $z_0 = \mathcal{E}(x)$, and a decoder $\mathcal{D}$ reconstructs $x \approx \mathcal{D}(z_0)$. During training, a forward process corrupts z_0 with Gaussian noise over T timesteps to produce z_t, and a conditional denoiser ϵ_θ is trained to predict the injected noise

$$\mathcal{L}_{\text{LDM}} = \mathbb{E}_{z_0,\, \epsilon\sim\mathcal{N}(0,I),\, t}\big[\, \|\epsilon - \epsilon_\theta(z_t, t, \tau(y))\|_2^2 \,\big], \quad (1)$$

where $\tau(y)$ denotes conditioning embeddings, such as text prompts extracted via a CLIP text encoder [35].

For completion tasks, generation is further conditioned on known visual context through a binary mask M, in which 1 marks given source pixels and 0 the region to synthesize. The reference latent $z_{\text{ref}} = z_0 \odot M$ is concatenated with z_t and M along the channel dimension, yielding $\hat{\epsilon} = \epsilon_\theta(z_t \oplus M \oplus z_{\text{ref}}, t, \tau(y))$. While effective for planar outpainting, this formulation does not account for the spherical geometry and periodic topology of omnidirectional imagery, which motivates our canonicalized framework.

3.2. The Omnidirectional Domain Gaps

To successfully integrate Euclidean ($\mathbb{R}^2$) generative priors with the spherical (S^2) omnidirectional manifold, our framework is dedicated to resolving two fundamental geometric discrepancies inherent to 360° generation.

Projective Variance. The mapping from a perspective image to the ERP canvas is determined by where the observation sits on the sphere. For in-the-wild inputs this spherical placement is unknown, and each placement induces a different distortion pattern in which straight world lines become sinusoidal curves. Such input-dependent distortion destabilizes the latent conditioning of LDMs, which implicitly rely on Manhattan-world regularities learned from perspective imagery. We resolve this by reformulating the generation target around a Canonical Viewing Space $\mathcal{C}$, a gravity-aligned frame in which the environmental vanishing line coincides with the ERP equator. Anchored to $\mathcal{C}$, the distortion no longer depends on the input placement and reduces to a fixed, predictable function of latitude. We thus seek a proxy transformation $\mathcal{T}_{\text{align}}$ that warps the input features into the canonical space, producing the canonical generative anchor

$$z_{\text{canonical}} = \mathcal{T}_{\text{align}}(z_{\text{ref}}). \quad (2)$$

Topological Severing. The ERP format inherently spans the azimuthal angle $\theta \in [-\pi, \pi]$, so its left and right boundaries depict physically adjacent content on the periodic S^1 boundary. Standard latent generative pipelines break this structure. Zero-padding during latent compression injects artificial borders, and absolute positional encodings in diffusion transformers treat opposite boundaries as maximally distant, which mathematically severs the S^1 periodic boundary and manifests as visible seams in the generated output. To mitigate this, our generative process is governed by strict Topological Equivariance, ensuring the network natively respects the continuous topology of the manifold.

3.3. Differentiable Projective Canonicalization

As established, our framework requires a proxy transformation $\mathcal{T}_{\text{align}}$ that anchors the unposed input to the Canonical Viewing Space $\mathcal{C}$. A natural choice is to train an unconstrained Spatial Transformer Network [19] end-to-end with the latent diffusion loss. However, $\mathcal{L}_{\text{LDM}}$ is dominated by high-frequency, pixel-level variations, and backpropagating such noisy gradients into a free-form warper induces non-rigid, "jelly-like" deformations rather than a coherent global alignment. Our Differentiable Projective Canonicalization (DPC) module avoids this failure mode by decoupling dense correspondence prediction from rigid geometric fitting.

Dense Correspondence Prediction. Given the perspective input I_p, a SegNeXt [13] encoder with a lightweight decoder predicts a dense correspondence field $\mathcal{P}_{\text{dense}} \in \mathbb{R}^{H_p \times W_p \times 2}$ that assigns to every input pixel its target coordinates on the canonical ERP canvas. Instead of regressing coordinates from scratch, the network predicts a bounded residual on top of the base grid of a canonical upright camera, and a ray-direction positional encoding is injected into the decoder so that the prediction remains aware of the underlying viewing geometry.

Differentiable Rigid Solver. Rather than warping features directly with $\mathcal{P}_{\text{dense}}$, we collapse it onto the 3-DoF manifold of rigid spherical cameras. We parameterize the camera as $\phi = (\theta_v, \theta_p, \theta_r)$, whose forward projection $f(\phi)$ maps perspective pixels onto the ERP canvas, and fit ϕ to the predicted field by nonlinear least squares:

$$\hat{\phi} \;=\; \arg\min_{\phi} \; \big\| f(\phi) - \mathcal{P}_{\text{dense}} \big\|_2^2, \quad (3)$$

solved with a closed-form Procrustes initialization followed by a few Levenberg–Marquardt iterations. From $\hat{\phi}$ we analytically reconstruct a *rigid coordinate grid*, which warps the input latent into $\mathcal{C}$ to form the canonical generative anchor:

$$z_{\text{canonical}} \;=\; \mathcal{W}(z_{\text{ref}},\, \hat{\phi}), \quad (4)$$

where $\mathcal{W}$ denotes differentiable grid sampling with the rigid coordinate grid.

Rigid Bottleneck as a Gradient Filter. By forcing the dense correspondence field to pass through the rigid bottleneck, the solver's Jacobian acts as a structural gradient filter during backpropagation. Because the rigid camera model has only three degrees of freedom, backpropagated gradients are projected onto the rank-3 subspace spanned by its Jacobian. Thus, noisy, spatially uncorrelated components of the diffusion gradient are suppressed, and only globally coherent, rigid alignment updates reach the dense predictor. This design prevents localized "jelly" warps while still allowing DPC to learn, jointly with the generator, the anchoring that best serves panorama completion.

3.4. Topologically Equivariant Generation

Having anchored the input features into $\mathcal{C}$, the remaining challenge is to synthesize the panorama without severing its periodic boundary. We enforce topological equivariance across both the compression and generation stages.

Circular Latent Encoding. We remove the artificial boundary at the compression stage without modifying the pre-trained VAE. Before encoding, the input is circularly pre-padded along the azimuthal axis, and the resulting latent is cropped back to its nominal extent afterwards. The convolutional receptive fields therefore wrap around the boundary while the frozen autoencoder weights and functionality remain untouched.

Siamese Shift-Equivariant Generation. Circular encoding provides the structural pathway for continuous feature propagation, but the generator must also be penalized for boundary-inconsistent predictions. Let $\mathrm{Roll}_\delta(\cdot)$ denote a circular shift along the azimuthal axis by a random offset δ. During training we perform two parallel prediction passes,

$$\hat{\epsilon}_{\text{base}} = \epsilon_\theta(z_t \oplus M \oplus z_{\text{canonical}},\, t,\, \tau(y)), \tag{5}$$

$$\hat{\epsilon}_{\text{shifted}} = \epsilon_\theta(\mathrm{Roll}_\delta(z_t \oplus M \oplus z_{\text{canonical}}),\, t,\, \tau(y)). \tag{6}$$

If the network models the underlying S^1 topology rather than overfitting to the Euclidean frame, shifting the base prediction by δ should agree with predicting from the shifted inputs. We penalize the discrepancy with a Siamese consistency loss

$$\mathcal{L}_{\text{shift}} = \mathbb{E}_{z_0,\epsilon,t,\delta}\big[\, \|\mathrm{Roll}_\delta(\hat{\epsilon}_{\text{base}}) - \hat{\epsilon}_{\text{shifted}}\|_2^2 \,\big]. \tag{7}$$

This objective enforces shift consistency in the latent space during denoising. By explicitly penalizing boundary-inconsistent generative logic, this formulation intrinsically binds the network to the continuous S^1 manifold. In practice, the learned consistency yields perceptually seamless outputs, which we quantify with seam-aware metrics in our experiments.

3.5. Overall Training Objective

The rigid bottleneck delivers a deliberately low-dimensional gradient to the dense predictor, which regularizes alignment but is insufficient as a sole training signal. We therefore anchor the dense correspondence field with direct supervision against the ground-truth correspondence $\mathcal{P}_{GT}$, analytically derived from the known sampling geometry of our canonicalized dataset,

$$\mathcal{L}_{\text{corr}} = \mathrm{SmoothL1}(\mathcal{P}_{\text{dense}},\, \mathcal{P}_{GT}). \tag{8}$$

The overall objective jointly minimizes the latent diffusion loss, the topological regularizer, and the geometric anchor,

$$\mathcal{L}_{\text{total}} = \mathcal{L}_{\text{LDM}} + \lambda_{\text{shift}}\mathcal{L}_{\text{shift}} + \lambda_{\text{corr}}\mathcal{L}_{\text{corr}}, \tag{9}$$

where λ_{shift} and λ_{corr} are scalar weights. Dense supervision provides the primary high-resolution signal for the correspondence field, while diffusion gradients arriving through the rigid bottleneck refine the anchoring toward placements that best serve completion, rather than accuracy alone.

4. The Horizon360 Dataset

Horizon360 constitutes the data level of our canonicalization. The structural prior that Gimbal360 learns is only as reliable as the canonical properties of its training panoramas, yet existing omnidirectional datasets [5, 49] frequently contain in-the-wild tilts and inconsistent horizon lines. Training a generative prior on such unrectified data contradicts the very constraints the Canonical Viewing Space is meant to provide. We therefore curate Horizon360, a large-scale panoramic dataset in which every environment satisfies the canonical constraints of $\mathcal{C}$.

Curation and Canonicalization. Horizon360 comprises 20k high-fidelity indoor and outdoor panoramic environments sourced from established open datasets [5, 10, 23, 51], web collections [34], and custom renders produced with Unreal Engine. Building on foundational omnidirectional geometric principles [54, 59], we adapt vanishing-point and zenith alignment strategies [20, 37, 38] to rectify every raw panorama, rotating the sphere so that the environmental vanishing line coincides with the ERP equator and physical plumb lines remain vertical. The resulting collection is gravity-aligned by construction.

Realistic Perspective Sampling. To train DPC and the canonicalized generator, we deploy a mixed sampling strategy that improves real-world robustness over standard uniform cropping [21, 42, 43]. Unlike prior works that fix the horizontal field of view, we drive sampling by the vertical

field of view θ_v and aspect ratio r, simulating diverse capture devices from wide-angle to telephoto through the effective focal lengths

$$f_y = \frac{1}{\tan(\theta_v/2)}, \qquad f_x = \frac{f_y}{r}. \tag{10}$$

Uniform sampling over-represents implausible extreme placements, while purely Gaussian sampling leaves the network brittle to outliers. We therefore draw the sampling parameters $\Theta = \{\theta_{\text{pitch}}, \theta_{\text{roll}}, \theta_v, r\}$ from a hybrid prior

$$P(\Theta) = \lambda \cdot \mathcal{N}(\mu_{\text{real}}, \sigma^2_{\text{real}}) + (1-\lambda) \cdot \mathcal{U}(\Theta_{\min}, \Theta_{\max}), \tag{11}$$

where $\lambda = 0.7$ focuses training on common, near-upright captures while retaining a 30% exposure to extreme placements, improving robustness to unconstrained user inputs.

Yaw-Centered Canonicalization. Finally, we decouple scene content from absolute heading. A circular permutation aligns the sampled view with the canonical center,

$$I_{\text{centered}} = \text{Roll}(I_{\text{ERP}}, -\psi_{\text{input}}), \tag{12}$$

so the model always receives conditioning at the center of the canvas and the wraparound boundary falls 180° behind the primary view. This simplification reduces boundary artifacts and stabilizes the topologically equivariant training of the generator.

5. Experiments

5.1. Experimental Settings

Implementation Details. Our model is built upon Flux.1-fill-dev [25] and fine-tuned with LoRA [16] on 8 GPUs for 10,000 steps with a batch size of 8, using AdamW with a constant learning rate of 1×10^{-4}. The training data comprises 20,000 panoramas from Horizon360, each producing three perspective samples under the hybrid prior of realistic sampling. We set the topological weight to $\lambda_{\text{shift}} = 0.5$ and the geometric weight to $\lambda_{\text{corr}} = 0.1$, balancing the auxiliary objectives against the diffusion loss.

Evaluation Protocol. For evaluation, we construct two held-out test sets: 5000 indoor images randomly sampled from Structured3D [58] and 5000 outdoor images from CVRG-Pano [33] and LayerPano3D [51], totaling 10,000 test images for comprehensive benchmarking. We measure visual quality with FID [15], KID [3], and FAED [53], and text alignment with CLIPScore [14]. To account for the spherical geometry and boundary continuity that these planar metrics fail to capture, we additionally report OmniFID (O-FID), which extends FID to the spherical domain through cubemap reprojection [7], and the Discontinuity Score (DS), which quantifies discontinuity across the periodic seam.

5.2. Main Results

We compare our method against HunyuanWorld 1.0 [18], WorldGen [50], and DiT360 [10], the strongest open-source methods built on the same Flux-fill backbone, which ensures that differences reflect the framework rather than the base model.

Quantitative Comparison. Tab. 1 reports results on both indoor and outdoor scenes. Our method achieves the best scores on all fidelity and geometry metrics, reducing FID over the strongest baseline WorldGen by 42% indoors and 40% outdoors, with comparable margins on KID, O-FID, and FAED. On the seam-specific DS, our score of 0.49 indoors nearly halves the best competing result, indicating that the improvements stem from structural and topological consistency rather than texture fidelity alone. CLIPScore varies only marginally across methods. DiT360 scores highest by a small margin yet exhibits the weakest structural fidelity and seam continuity, suggesting that text adherence alone does not translate into coherent panoramas.

Qualitative Comparison Fig. 3 compares panoramic completions on indoor and outdoor scenes, where dashed outlines mark corresponding regions across methods and are magnified in the side insets. Gimbal360 anchors each unposed input at its canonical frame, so the completed environments exhibit the correct latitude-dependent distortion profile, straight structural lines, and coherent global layout. HunyuanWorld projects inputs with fixed viewing parameters and thus inherits a mismatched distortion profile, bending structures around the conditioning region. WorldGen reduces these errors yet retains local structural drift and occasional discontinuities at the periodic boundary, and DiT360 fails to preserve the input region and exhibits severe structural inconsistency. The magnified crops further show that our canonicalized completions preserve structural regularity and remain coherent in both scene content and layout. Moreover, our method surpasses all competing baselines in synthesizing continuous content across the seam, without resorting to post-hoc blending.

In-the-Wild Generalization. Fig. 4 evaluates zero-shot robustness on in-the-wild inputs outside the training distribution, spanning real indoor photographs with unknown viewing geometry and stylized illustrations with various aspect ratios. Gimbal360 anchors each input in the canonical viewing space to better leverage the internalized generative priors. Thus, the completions remain faithful to the conditioning in structure, semantics, and visual style, extending the illustrated scene with a plausible global layout. Competing methods instead surround the input with content of mismatched scale or semantics, wash out the scene identity, or

Method	Indoor, 5K						Outdoor, 5K					
	FID↓	KID($\times 10^2$)↓	O-FID↓	FAED↓	CS↑	DS↓	FID↓	KID($\times 10^2$)↓	O-FID↓	FAED↓	CS↑	DS↓
HunyuanWorld 1.0	29.23	2.1981	53.26	4.05	26.48	0.92	41.37	2.2218	69.44	7.07	29.13	1.00
WorldGen	27.43	1.9683	50.50	2.45	26.44	1.32	39.78	2.0616	67.47	6.47	29.10	1.01
DiT360	38.43	3.4848	70.61	11.30	**31.09**	3.76	55.17	3.7295	65.56	8.35	**31.40**	2.08
Ours	**15.92**	**1.0249**	**30.10**	**1.36**	30.68	**0.49**	**23.78**	**0.9228**	**47.48**	**1.75**	31.29	**0.66**

Table 1. Quantitative comparison on both indoor and outdoor scenes, with 5,000 held-out samples per domain. KID is scaled by 10^2. Bold marks the best result.

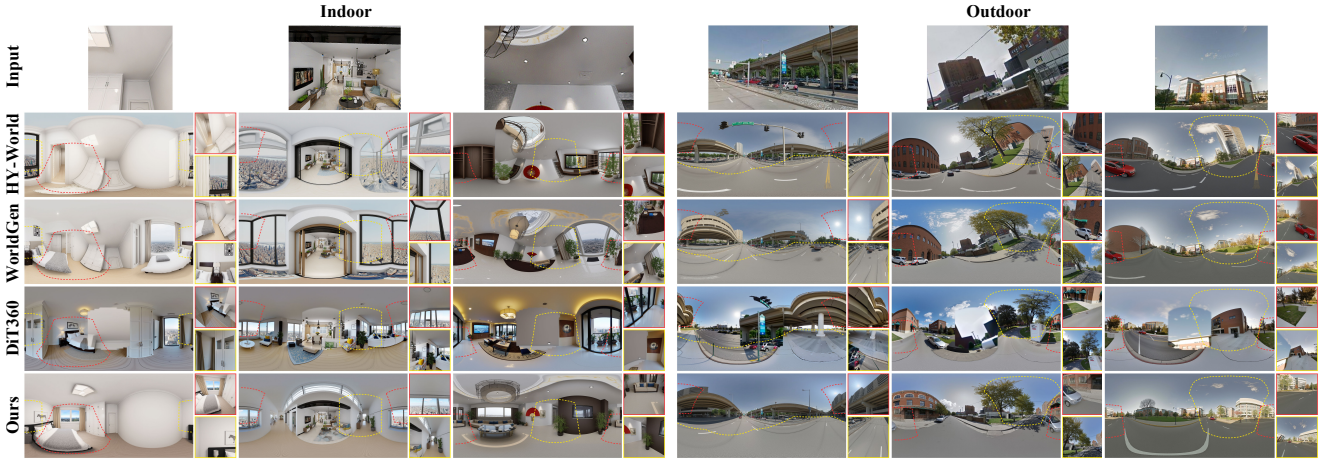


Figure 3. Qualitative comparison on indoor (left) and outdoor (right) scenes. Baseline completions exhibit warped structures, mismatched distortion profiles, and boundary discontinuities, whereas ours completes structurally coherent, boundary-continuous panoramas. Please zoom in for details.



Figure 4. Qualitative results of in-the-wild generalization. Inputs include real-world captures and styled photos. Competing methods produce mismatched surroundings or warped layouts, whereas Gimbal360 completes structure- and style-consistent panoramas. Please zoom in for details.

warp the global layout, as highlighted by the dashed regions and magnified crops. These support the practical utility of our canonicalized completion for unconstrained inputs.

Method	Indoor, 0.5K				Outdoor, 0.5K			
	FID↓	KID ↓	O-FID↓	DS↓	FID↓	KID ↓	O-FID↓	DS↓
w/o DPC	64.48	1.2716	93.03	1.63	69.82	1.9039	108.00	1.09
Geocalib	70.50	1.3122	100.27	1.10	78.93	2.1227	112.35	0.98
PF	72.54	1.3640	102.36	0.99	81.25	2.5321	116.56	0.94
w/o TEG	55.05	0.8106	79.49	1.75	**62.74**	**0.8194**	106.62	1.49
Ours	**54.18**	**0.8012**	**79.45**	**0.51**	63.28	0.8236	**99.04**	**0.69**

Table 2. Ablation study and anchoring baselines. Geocalib and PF denote replacing DPC with GeoCalib [43] and Perspective-Fields [21], respectively, while keeping TEG fixed. Bold marks the best result. KID is scaled by 10^2.

5.3. Ablation Studies

We ablate on a subset of 500 images per domain sampled from our test sets, comparing five variants under identical settings. *w/o DPC* removes the geometric module, projecting the input with fixed viewing parameters and forcing the generator to resolve projective variance implicitly. *w/o TEG*



Figure 5. Qualitative ablation results. Removing DPC yields severe structural distortion while removing TEG breaks continuity near the periodic boundary. Our full model produces structurally coherent and boundary-continuous completions.

keeps DPC but trains with standard latent encoding and no shift-equivariance objective. *Geocalib* and *PF* replace DPC with the external estimators GeoCalib [43] and PerspectiveFields [21], whose predicted parameters drive the projection while TEG remains active. *Ours* is the full model. Quantitative and qualitative results are reported in Tab. 2 and Fig. 5.

Effect of DPC. Removing DPC degrades every metric, with indoor FID rising from 54.18 to 64.48 and outdoor O-FID from 99.04 to 108.00, and yields severe structural distortion. More importantly, both Geocalib and PF recover plausible placements, yet completion quality drops markedly, with indoor FID rising to 70.50 and 72.54 respectively. This indicates that a geometrically accurate placement is not necessarily the one that best serves completion. Trained jointly with the generator, DPC learns the anchoring that minimizes downstream synthesis error, which makes it an integral component rather than a swappable preprocessing step.

Effect of TEG. Removing TEG leaves FID nearly unchanged, and the ablated variant even attains a marginally lower outdoor FID. This is expected since FID is insensitive to the periodic boundary. The seam-specific DS reveals the actual contribution, dropping from 1.75 to 0.51 indoors and from 1.49 to 0.69 outdoors once TEG is enabled. These gains indicate that circular latent encoding and the Siamese objective enforce a continuity that post-hoc corrections cannot achieve, and that the two mechanisms complement each other, with the full model achieving the best overall results.

6. Conclusion

We presented Gimbal360, a framework for completing 360° panoramas from a single unposed perspective image by explicitly addressing the geometric and topological mismatch between Euclidean diffusion priors and spherical panoramas. By introducing a Canonical Viewing Space, a Differentiable Projective Canonicalization module for anchoring inputs, and a topologically equivariant generation strategy that preserves the intrinsic S^1 periodicity, our method produces structurally consistent and seamless omnidirectional completions.

References

[1] Naofumi Akimoto, Yuhi Matsuo, and Yoshimitsu Aoki. Diverse plausible 360-degree image outpainting for efficient 3dcg background creation. In *CVPR*, pages 11441–11450, 2022. 2

[2] Shuai Bai, Yuxuan Cai, Ruizhe Chen, Keqin Chen, Xionghui Chen, Zesen Cheng, Lianghao Deng, Wei Ding, Chang Gao, Chunjiang Ge, Wenbin Ge, Zhifang Guo, Qidong Huang, Jie Huang, Fei Huang, Binyuan Hui, Shutong Jiang, Zhaohai Li, Mingsheng Li, Mei Li, Kaixin Li, Zicheng Lin, Junyang Lin, Xuejing Liu, Jiawei Liu, Chenglong Liu, Yang Liu, Dayiheng Liu, Shixuan Liu, Dunjie Lu, Ruilin Luo, Chenxu Lv, Rui Men, Lingchen Meng, Xuancheng Ren, Xingzhang Ren, Sibo Song, Yuchong Sun, Jun Tang, Jianhong Tu, Jianqiang Wan, Peng Wang, Pengfei Wang, Qiuyue Wang, Yuxuan Wang, Tianbao Xie, Yiheng Xu, Haiyang Xu, Jin Xu, Zhibo Yang, Mingkun Yang, Jianxin Yang, An Yang, Bowen Yu, Fei Zhang, Hang Zhang, Xi Zhang, Bo Zheng, Humen Zhong, Jingren Zhou, Fan Zhou, Jing Zhou, Yuanzhi Zhu, and Ke Zhu. Qwen3-vl technical report. *arXiv preprint arXiv:2511.21631*, 2025. 11

[3] Mikołaj Bińkowski, Danica J Sutherland, Michael Arbel, and Arthur Gretton. Demystifying mmd gans. In *International Conference on Learning Representations*, 2018. 6

[4] Hakan Çapuk, Andrew Bond, Muhammed Burak Kızıl, Emir Göçen, Erkut Erdem, and Aykut Erdem. Tandit: Tangent-plane diffusion transformer for high-quality 360 {\deg} panorama generation. *arXiv preprint arXiv:2506.21681*, 2025. 3

[5] Angel Chang, Angela Dai, Thomas Funkhouser, Maciej Halber, Matthias Niebner, Manolis Savva, Shuran Song, Andy Zeng, and Yinda Zhang. Matterport3d: Learning from rgb-d data in indoor environments. In *2017 International Conference on 3D Vision (3DV)*, pages 667–676. IEEE Computer Society, 2017. 5

[6] Zhaoxi Chen, Guangcong Wang, and Ziwei Liu. Text2light: Zero-shot text-driven hdr panorama generation. *ACM TOG*, 41(6):1–16, 2022. 2

[7] Anders Christensen, Nooshin Mojab, Khushman Patel, Karan Ahuja, Zeynep Akata, Ole Winther, Mar Gonzalez-Franco, and Andrea Colaco. Geometry fidelity for spherical images. In *European Conference on Computer Vision*, pages 276–292. Springer, 2024. 6

[8] Benjamin Coors, Alexandru Paul Condurache, and Andreas Geiger. Spherenet: Learning spherical representations for detection and classification in omnidirectional images. In *ECCV*, pages 518–533, 2018. 3

[9] Patrick Esser, Sumith Kulal, Andreas Blattmann, Rahim Entezari, Jonas Müller, Harry Saini, Yam Levi, Dominik Lorenz, Axel Sauer, Frederic Boesel, et al. Scaling rectified flow transformers for high-resolution image synthesis. In *ICML*, 2024. 2

[10] Haoran Feng, Dizhe Zhang, Xiangtai Li, Bo Du, and Lu Qi. Dit360: High-fidelity panoramic image generation via hybrid training. *arXiv preprint arXiv:2510.11712*, 2025. 3, 5, 6

[11] Mengyang Feng, Jinlin Liu, Miaomiao Cui, and Xuansong Xie. Diffusion360: Seamless 360 degree panoramic image generation based on diffusion models. *arXiv preprint arXiv:2311.13141*, 2023. 2, 3

[12] Ian Goodfellow, Jean Pouget-Abadie, Mehdi Mirza, Bing Xu, David Warde-Farley, Sherjil Ozair, Aaron Courville, and Yoshua Bengio. Generative adversarial networks. *Communications of the ACM*, 63(11):139–144, 2020. 2

[13] Meng-Hao Guo, Cheng-Ze Lu, Qibin Hou, Zhengning Liu, Ming-Ming Cheng, and Shi-Min Hu. Segnext: Rethinking convolutional attention design for semantic segmentation. *NeurIPS*, 35:1140–1156, 2022. 4

[14] Jack Hessel, Ari Holtzman, Maxwell Forbes, Ronan Le Bras, and Yejin Choi. Clipscore: A reference-free evaluation metric for image captioning. In *Proceedings of the 2021 conference on empirical methods in natural language processing*, pages 7514–7528, 2021. 6

[15] Martin Heusel, Hubert Ramsauer, Thomas Unterthiner, Bernhard Nessler, and Sepp Hochreiter. Gans trained by a two time-scale update rule converge to a local nash equilibrium. *Advances in neural information processing systems*, 30, 2017. 6

[16] Edward J Hu, Yelong Shen, Phillip Wallis, Zeyuan Allen-Zhu, Yuanzhi Li, Shean Wang, Liang Wang, Weizhu Chen, et al. Lora: Low-rank adaptation of large language models. *Iclr*, 1(2):3, 2022. 6, 11

[17] Yukun Huang, Yanning Zhou, Jianan Wang, Kaiyi Huang, and Xihui Liu. Dreamcube: 3d panorama generation via multi-plane synchronization. *arXiv preprint arXiv:2506.17206*, 2025. 3

[18] Team HunyuanWorld. Hunyuanworld 1.0: Generating immersive, explorable, and interactive 3d worlds from words or pixels. *arXiv preprint*, 2025. 2, 3, 6, 16

[19] Max Jaderberg, Karen Simonyan, Andrew Zisserman, et al. Spatial transformer networks. *NeurIPS*, 28, 2015. 2, 4

[20] Zhigang Jiang, Zhongzheng Xiang, Jinhua Xu, and Ming Zhao. Lgt-net: Indoor panoramic room layout estimation with geometry-aware transformer network. In *CVPR*, pages 1654–1663, 2022. 5

[21] Linyi Jin, Jianming Zhang, Yannick Hold-Geoffroy, Oliver Wang, Kevin Blackburn-Matzen, Matthew Sticha, and David F Fouhey. Perspective fields for single image camera calibration. In *CVPR*, pages 17307–17316, 2023. 5, 7, 8

[22] Nikolai Kalischek, Michael Oechsle, Fabian Manhardt, Philipp Henzler, Konrad Schindler, and Federico Tombari. Cubediff: Repurposing diffusion-based image models for panorama generation. In *ICLR*, 2025. 3

[23] Muhammed Kocabas, Chun-Hao P Huang, Joachim Tesch, Lea Müller, Otmar Hilliges, and Michael J Black. Spec: Seeing people in the wild with an estimated camera. In *ICCV*, pages 11035–11045, 2021. 5

[24] Theodoros Kouzelis, Ioannis Kakogeorgiou, Spyros Gidaris, and Nikos Komodakis. Eq-vae: Equivariance regularized latent space for improved generative image modeling. In *International Conference on Machine Learning*, pages 31648–31666. PMLR, 2025. 13

[25] Black Forest Labs. Flux. https://github.com/black-forest-labs/flux, 2024. 2, 6, 11

[26] Yuseung Lee, Kunho Kim, Hyunjin Kim, and Minhyuk Sung. Syncdiffusion: Coherent montage via synchronized joint diffusions. *NeurIPS*, 36:50648–50660, 2023. 2, 3

[27] Jialu Li and Mohit Bansal. Panogen: Text-conditioned panoramic environment generation for vision-and-language navigation. *NeurIPS*, 36:21878–21894, 2023. 2

[28] Kang Liao, Xiangyu Xu, Chunyu Lin, Wenqi Ren, Yunchao Wei, and Yao Zhao. Cylin-painting: Seamless 360 panoramic image outpainting and beyond. *IEEE TIP*, 33: 382–394, 2023. 3

[29] Aoming Liu, Zhong Li, Zhang Chen, Nannan Li, Yi Xu, and Bryan A Plummer. Panofree: Tuning-free holistic multi-view image generation with cross-view self-guidance. In *ECCV*, pages 146–164. Springer, 2024. 3

[30] Yuanxun Lu, Jingyang Zhang, Tian Fang, Jean-Daniel Nahmias, Yanghai Tsin, Long Quan, Xun Cao, Yao Yao, and Shiwei Li. Matrix3d: Large photogrammetry model all-in-one. In *CVPR*, pages 11250–11263, 2025. 2, 3

[31] Andreas Lugmayr, Martin Danelljan, Andres Romero, Fisher Yu, Radu Timofte, and Luc Van Gool. Repaint: Inpainting using denoising diffusion probabilistic models. In *CVPR*, pages 11461–11471, 2022. 2

[32] Changgyoon Oh, Wonjune Cho, Yujeong Chae, Daehee Park, Lin Wang, and Kuk-Jin Yoon. Bips: Bi-modal indoor panorama synthesis via residual depth-aided adversarial learning. In *ECCV*, pages 352–371. Springer, 2022. 2

[33] Semih Orhan and Yalin Bastanlar. Semantic segmentation of outdoor panoramic images. *Signal, Image and Video Processing*, 2021. 6

[34] Poly Haven. Poly haven hdris. https://polyhaven.com/hdris. Accessed: December 2025. 5

[35] Alec Radford, Jong Wook Kim, Chris Hallacy, Aditya Ramesh, Gabriel Goh, Sandhini Agarwal, Girish Sastry, Amanda Askell, Pamela Mishkin, Jack Clark, et al. Learning transferable visual models from natural language supervision. In *ICML*, pages 8748–8763. PmLR, 2021. 4

[36] Robin Rombach, Andreas Blattmann, Dominik Lorenz, Patrick Esser, and Björn Ommer. High-resolution image synthesis with latent diffusion models. In *CVPR*, pages 10684–10695, 2022. 1, 2, 4

[37] Cheng Sun, Chi-Wei Hsiao, Min Sun, and Hwann-Tzong Chen. Horizonnet: Learning room layout with 1d represen-

tation and pano stretch data augmentation. In *CVPR*, pages 1047–1056, 2019. 5

[38] Cheng Sun, Min Sun, and Hwann-Tzong Chen. Hohonet: 360 indoor holistic understanding with latent horizontal features. In *CVPR*, pages 2573–2582, 2021. 5

[39] Xiancheng Sun, Senmao Ma, Shengxi Li, Mai Xu, Jingyuan Xia, Lai Jiang, Xin Deng, and Jiali Wang. Spherical-nested diffusion model for panoramic image outpainting. In *ICML*, 2025. 3

[40] Xiancheng Sun, Mai Xu, Shengxi Li, Senmao Ma, Xin Deng, Lai Jiang, and Gang Shen. Spherical manifold guided diffusion model for panoramic image generation. In *CVPR*, pages 5824–5834, 2025. 3

[41] Jing Tan, Shuai Yang, Tong Wu, Jingwen He, Yuwei Guo, Ziwei Liu, and Dahua Lin. Imagine360: Immersive 360 video generation from perspective anchor. *arXiv preprint arXiv:2412.03552*, 2024. 3

[42] Javier Tirado-Garín and Javier Civera. Anycalib: On-manifold learning for model-agnostic single-view camera calibration. In *ICCV*, pages 8044–8055, 2025. 5

[43] Alexander Veicht, Paul-Edouard Sarlin, Philipp Lindenberger, and Marc Pollefeys. Geocalib: Learning single-image calibration with geometric optimization. In *ECCV*, pages 1–20. Springer, 2024. 5, 7, 8

[44] Qian Wang, Weiqi Li, Chong Mou, Xinhua Cheng, and Jian Zhang. 360dvd: Controllable panorama video generation with 360-degree video diffusion model. In *CVPR*, pages 6913–6923, 2024. 3

[45] Yi Wang, Xin Tao, Xiaoyong Shen, and Jiaya Jia. Wide-context semantic image extrapolation. In *CVPR*, pages 1399–1408, 2019. 2

[46] World Labs. Generating worlds. https://www.worldlabs.ai/blog/generating-worlds, 2026. Accessed: February 2026. 2, 16

[47] Tao Wu, Xuewei Li, Zhongang Qi, Di Hu, Xintao Wang, Ying Shan, and Xi Li. Spherediffusion: Spherical geometry-aware distortion resilient diffusion model. In *AAAI*, pages 6126–6134, 2024. 3

[48] Tianhao Wu, Chuanxia Zheng, and Tat-Jen Cham. Panodiffusion: 360-degree panorama outpainting via diffusion. In *ICLR*, 2024. 2, 3

[49] Jianxiong Xiao, Krista A Ehinger, Aude Oliva, and Antonio Torralba. Recognizing scene viewpoint using panoramic place representation. In *CVPR*, pages 2695–2702. IEEE, 2012. 5

[50] Ziyang Xie. Worldgen: Generate any 3d scene in seconds. https://github.com/ZiYang-xie/WorldGen, 2025. 6, 16

[51] Shuai Yang, Jing Tan, Mengchen Zhang, Tong Wu, Gordon Wetzstein, Ziwei Liu, and Dahua Lin. Layerpano3d: Layered 3d panorama for hyper-immersive scene generation. In *Proceedings of the special interest group on computer graphics and interactive techniques conference conference papers*, pages 1–10, 2025. 5, 6

[52] Xiaoding Yuan, Shitao Tang, Kejie Li, and Peng Wang. Camfreediff: camera-free image to panorama generation with diffusion model. In *CVPR*, pages 16408–16417, 2025. 3

[53] Cheng Zhang, Qianyi Wu, Camilo Cruz Gambardella, Xiaoshui Huang, Dinh Phung, Wanli Ouyang, and Jianfei Cai. Taming stable diffusion for text to 360 panorama image generation. In *CVPR*, pages 6347–6357, 2024. 3, 6

[54] Yinda Zhang, Shuran Song, Ping Tan, and Jianxiong Xiao. Panocontext: A whole-room 3d context model for panoramic scene understanding. In *ECCV*, pages 668–686. Springer, 2014. 5

[55] Shengyu Zhao, Jonathan Cui, Yilun Sheng, Yue Dong, Xiao Liang, Eric I Chang, and Yan Xu. Large scale image completion via co-modulated generative adversarial networks. *arXiv preprint arXiv:2103.10428*, 2021. 2

[56] Chuanxia Zheng, Tat-Jen Cham, and Jianfei Cai. Pluralistic image completion. In *CVPR*, pages 1438–1447, 2019. 2

[57] Dian Zheng, Cheng Zhang, Xiao-Ming Wu, Cao Li, Chengfei Lv, Jian-Fang Hu, and Wei-Shi Zheng. Panorama generation from nfov image done right. In *CVPR*, pages 21610–21619, 2025. 2, 3

[58] Jia Zheng, Junfei Zhang, Jing Li, Rui Tang, Shenghua Gao, and Zihan Zhou. Structured3d: A large photo-realistic dataset for structured 3d modeling. In *ECCV*, 2020. 6

[59] Chuhang Zou, Alex Colburn, Qi Shan, and Derek Hoiem. Layoutnet: Reconstructing the 3d room layout from a single rgb image. In *CVPR*, pages 2051–2059, 2018. 5

Gimbal360: Canonicalizing Planar Diffusion for Spherical Panorama Completion

Supplementary Material

This supplementary document provides extended technical details, comprehensive qualitative evaluations, and dataset curation methodologies. Sec. A provides both training and inference details. Sec. B elaborates on the curation, canonicalization, and captioning of the Horizon360 dataset. Sec. C presents an analysis of our Siamese shift-equivariance objective on the S^1 boundary, followed by our efficient positional-encoding-based implementation. Sec. D presents additional qualitative results and a discussion of limitations.

A. Extended Experimental Setups

A.1. Training Details

To fine-tune Gimbal360 while managing the memory footprint of the Flux.1-fill-dev backbone [25], we apply LoRA [16] to the attention matrices (query, key, value) and feed-forward networks of the frozen transformer blocks, with rank $r = 64$ and scaling $\alpha = 64$. Target panoramas are processed at an ERP resolution of 960×1920.

The pre-trained VAE remains entirely frozen. We do not modify its layers or weights. Continuity across the S^1 boundary is instead obtained by circularly pre-padding the input along the azimuthal axis before encoding and cropping the latent back to its nominal extent afterwards, so the convolutional receptive fields wrap around the boundary while the pre-trained latent distribution is preserved.

The overall objective jointly minimizes the diffusion loss, the topological Siamese regularizer, and the geometric correspondence anchor, with $\lambda_{\text{shift}} = 0.5$ and $\lambda_{\text{corr}} = 0.1$ balancing the auxiliary gradients against the diffusion loss. Training runs on 4 NVIDIA H20 GPUs with PyTorch 2.7.0.

A.2. Inference Details

We use the Euler sampler for 30 denoising steps with a classifier-free guidance scale of 30.0, the default configuration of Flux-fill. To exploit the learned shift equivariance, we apply a random circular shift δ_t to the latent at each denoising step and let the spatial frame translate continuously along the generative trajectory, so the Euclidean border of the latent tensor is repositioned across the S^1 boundary throughout sampling and no static seam can form. After the final step, a single inverse shift compensates the accumulated translation and realigns the latent with the canonical conditioning, and the result is decoded with the circular-padded VAE decoder.

B. Horizon360 Dataset Details

B.1. Curation and Captioning

Horizon360 comprises 20k high-fidelity panoramic environments aggregated from open-source repositories and high-quality synthetic renders, spanning complex indoor scenes with intricate lighting and dense geometric structure as well as expansive outdoor scenarios. Text prompts are generated with a vision–language model (e.g., Qwen3-VL [2]) from the canonicalized panoramas. Fig. 6 shows a random selection of canonicalized ground-truth panoramas, illustrating the diversity of the dataset.

B.2. Canonicalization

Every panorama is rectified prior to training. As illustrated in Fig. 7, raw unaligned panoramas exhibiting sinusoidal distortions are rotated on the sphere so that the true horizon aligns with the geometric equator of the ERP and vertical lines are rendered plumb, providing the gravity-aligned structural prior required by the Canonical Viewing Space.

B.3. Mixture-Distribution Pose Sampling

To improve robustness on unposed, in-the-wild photographs, we sample perspective crops that simulate realistic captures. Real user photos mix small hand-held jitter with occasional extreme, intentional angles, which neither a pure Gaussian nor a pure uniform prior captures. We therefore sample each parameter with a mixture-distribution strategy:

- **Yaw.** Sampled uniformly over $(-\pi, \pi)$ for unbiased azimuthal coverage.
- **Pitch.** 70% from $\mathcal{N}(0, 15^\circ)$ simulating eye-level photography and 30% from $\mathcal{U}(-45^\circ, 45^\circ)$ covering extreme upward and downward shots.
- **Roll.** 80% from $\mathcal{N}(0, 5^\circ)$ simulating handheld instability and 20% from $\mathcal{U}(-45^\circ, 45^\circ)$ covering aggressive tilt.
- **Field of view.** 80% from $\mathcal{N}(60^\circ, 10^\circ)$ and 80% from $\mathcal{U}(45^\circ, 100^\circ)$, covering wide-angle to telephoto optics.

C. Topological Equivariance

The main paper introduces a Siamese shift-equivariance objective for Topologically Equivariant Generation (TEG) that natively governs the diffusion process. Here we analyze the conditions under which this objective yields shift-equivariant denoising on the S^1 boundary, and then describe our memory-efficient implementation via positional-encoding manipulation.



Figure 6. **Horizon360 Dataset Diversity.** A representative sample of our curated, gravity-aligned panoramas. The dataset spans a wide domain of indoor structures and outdoor landscapes under diverse lighting conditions, providing a robust, generalized training signal for the Gimbal360 framework.

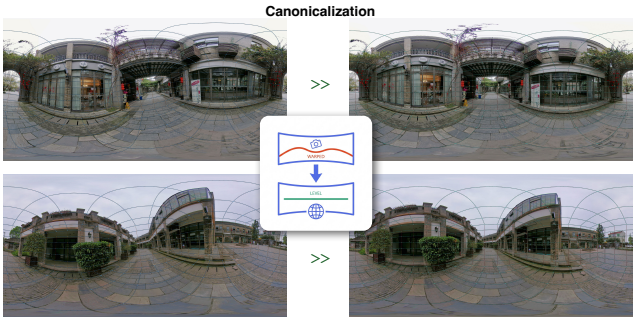


Figure 7. **Dataset Canonicalization.** Visualization of the rectification process applied to Horizon360. Raw unaligned panoramas (left) exhibiting severe sinusoidal distortions are mathematically rotated into the Canonical Viewing Space (right), ensuring a perfectly straight equator and plumb architectural verticals.

C.1. Problem Formulation and S^1 Topology

Let $Z \in \mathbb{R}^{C\times H\times W}$ denote the latent of an ERP panorama, where W spans the azimuth $\theta \in [-\pi, \pi]$. A true omnidirectional environment lies on S^2, and its cylindrical projection onto the azimuthal axis forms a periodic S^1 boundary. Mathematically, this enforces a strict boundary condition for any integer k:

$$Z[:, :, w] \equiv Z[:, :, (w + k \cdot W) \bmod W].$$

Standard latent diffusion architectures violate this condition through bounded spatial priors that treat $w = 0$ and $w = W - 1$ as maximally distant.

C.2. Equivariance under the Siamese Objective

We define the circular translation operator Roll_δ with $[\mathrm{Roll}_\delta(Z)]_{:,:,w} = Z_{:,:,(w-\delta) \bmod W}$, which shifts a ten-



Figure 8. Out-of-Distribution Generalization.

sor along the azimuthal axis W by an integer offset $\delta \in [0, W-1]$. With combined input $X = z_t \oplus M \oplus z_{\text{canonical}}$, the Siamese objective minimizes

$$\mathcal{L}_{\text{shift}} = \mathbb{E}_{X,t,\delta}\big[\, \|\text{Roll}_\delta(\epsilon_\theta(X,t)) - \epsilon_\theta(\text{Roll}_\delta(X),t)\|_2^2 \,\big].$$

In the limit $\mathcal{L}_{\text{shift}} \to 0$, the properties of the L_2 norm imply $\text{Roll}_\delta(\epsilon_\theta(X,t)) = \epsilon_\theta(\text{Roll}_\delta(X),t)$ almost everywhere, so the denoiser's prediction cannot depend on the absolute azimuthal coordinate. Had the network learned an artificial boundary feature at a fixed position (e.g., a seam at $w = 0$), shifting the input would move the content while the artifact remained static, violating this equality. The objective therefore drives the denoiser to process the latent as a closed loop along the azimuth.

Two caveats bound this analysis. It holds in the limit of a converged Siamese loss rather than unconditionally, and it constrains the denoiser in latent space. Since pre-trained autoencoders are not in general equivariant under spatial transformations [24], latent-space consistency does not formally transfer to the pixel domain. Empirically, the learned consistency yields perceptually seamless decoded outputs, which the seam-specific metrics quantifies.

C.3. Efficient Implementation via Positional Shifting

Physically rolling high-dimensional latent concatenations in memory at every training step introduces avoidable overhead.Because diffusion transformers process images as sequences of tokens whose spatial structure is injected purely through the positional encoding $P(x, y)$, a circular shift of the image tensor is mathematically identical to an inverse circular shift of the positional encodings,

$$P_{\text{shifted}}(x, y) = P((x - \delta) \bmod W,\, y).$$

During training, the base branch processes the canonical inputs with the default coordinate grid, while the shifted branch processes the identical unshifted tensor conditioned on the circularly shifted encodings. The fast memory-level Roll_δ is applied only to the base branch's output to align the two predictions for the L_2 penalty, avoiding duplicate memory allocation for the inputs. At inference, the denoiser runs

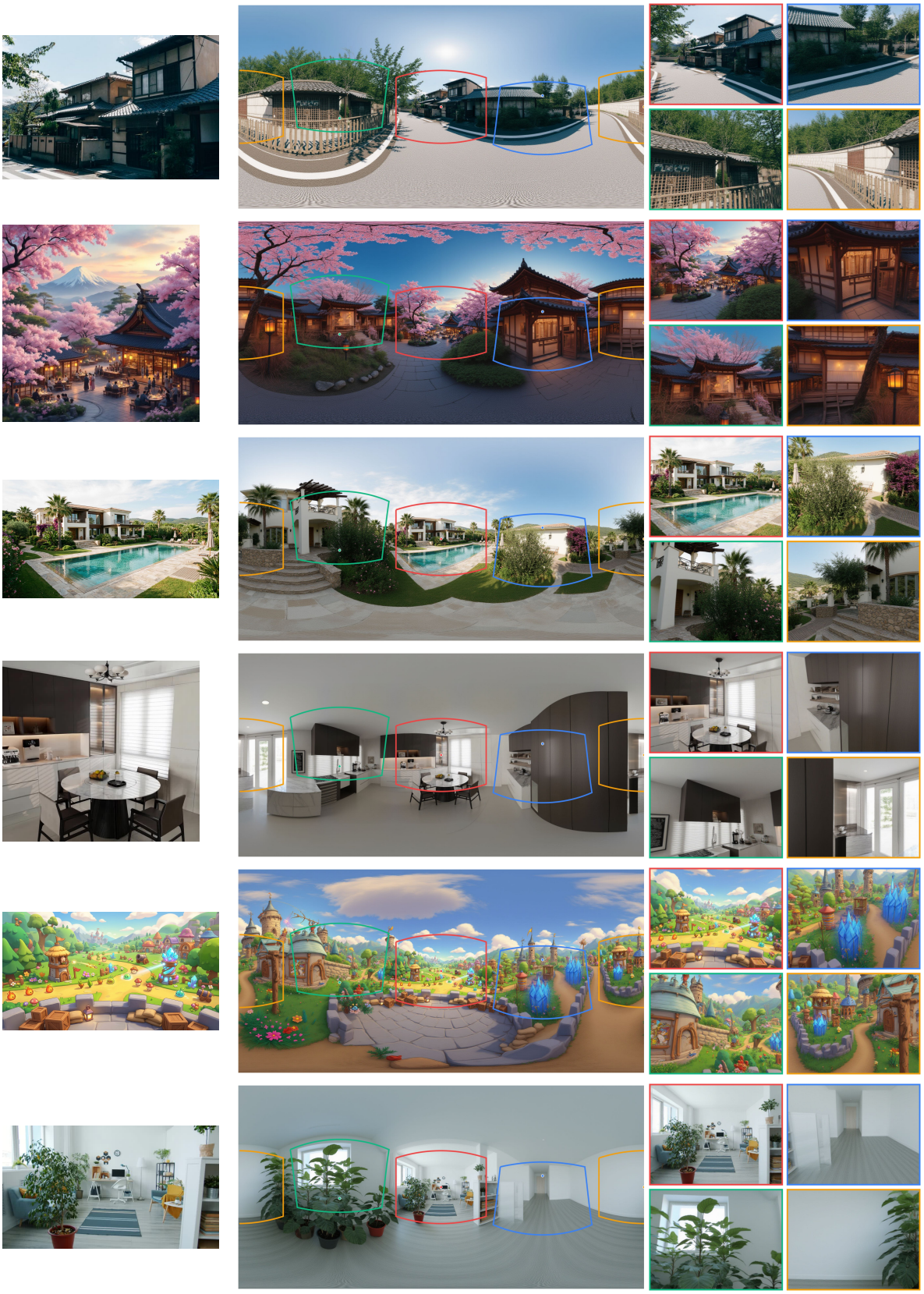


Figure 9. Out-of-Distribution Generalization.

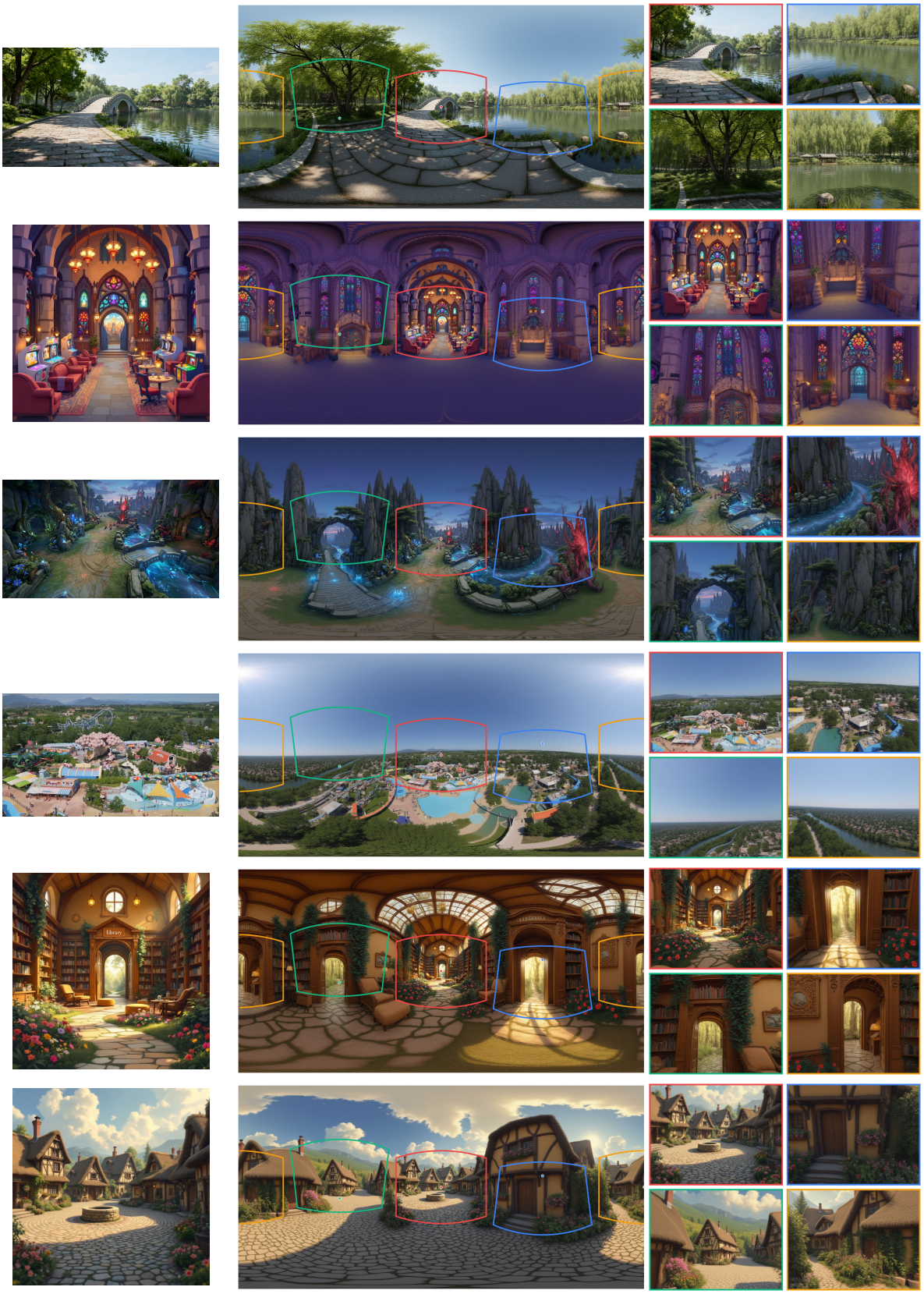


Figure 10. Out-of-Distribution Generalization.

a single forward pass per step, exactly as in the standard pipeline. The random per-step shift δ_t described in Sec. A amounts to one circular index remapping per step, applied either to the latent directly or, equivalently, to its positional encodings, and a single inverse shift realigns the final latent before decoding. TEG therefore adds no additional network evaluations and negligible overhead at inference.

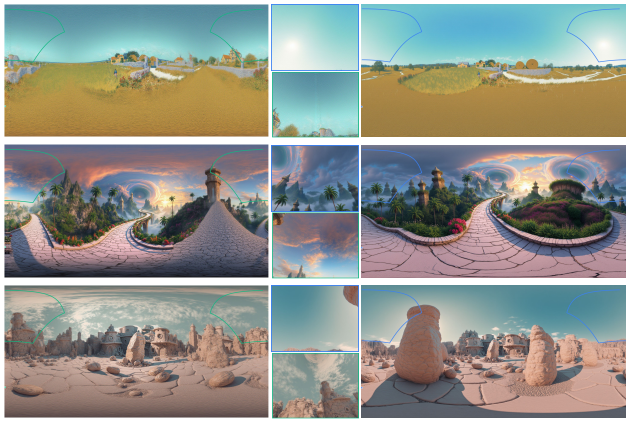


Figure 11. **Boundary Continuity Comparison.** A zoomed-in analysis of the S^1 azimuthal seam. Baseline method (left) relying on inference-time circular blending suffer from unnatural texture smoothing and relocated secondary seams at the blend edges. Gimbal360 (right) natively generates seamless boundaries with preserved high-frequency details and structural integrity.



Figure 12. **Limitations and Failure Cases.** (Top) Generation with humans leads to inaccurate anatomical distortions. (Bottom) An extreme telephoto input (right) provides insufficient context, occasionally resulting in completion with less coherent global geometry than a wide-angled input (left).

D. Additional Qualitative Results

D.1. Out-of-Distribution Generalization

We test Gimbal360 on challenging out-of-distribution inputs collected from the evaluation suites of contemporaneous works [18, 46, 50], together with self-collected smartphone captures and AI-generated images. These inputs feature unconstrained environments and artistic lighting that deviate substantially from Horizon360. As shown in Fig. 8, 9, and 10, Gimbal360 anchors these inputs into the Canonical Viewing Space and completes geometrically plausible, immersive 360° environments.

D.2. Seamless Synthesis at the S^1 Boundary

Fig. 11 compares zoomed-in boundary regions against WorldGen [50]. Methods that rely on inference-time circular blending exhibit two characteristic artifacts. Averaging conflicting values across the boundary destroys high-frequency detail, producing smoothed or ghosted textures at the seam, and the abrupt transition at the edge of the blending zone often relocates the seam to a new position rather than removing it. In contrast, Gimbal360 enforces continuous spatial logic during generation through TEG, yielding perceptually seamless boundaries with preserved high-frequency detail and structural coherence, without any destructive inference-time blending.

D.3. Limitations and Failure Cases

Fig.12 illustrates two primary limitations rooted in single-view geometry and latent diffusion priors. When the input is heavily dominated by human subjects, synthesizing articulated anatomy under ERP distortion remains challenging for the diffusion prior, occasionally producing unnatural scaling and unsatisfactory results with severely distorted figures. Additionally, extreme telephoto inputs provide little structural context to anchor a full environment, forcing the prior to hallucinate most of the canvas with minimal conditioning, which can degrade global layout coherence and fidelity.